Eur. Phys. J. D **1**, 71–78 (1998)

THE EUROPEAN PHYSICAL JOURNAL D

Rotational effects in low energy dissociative recombination of diatomic ions

B. Vâlcu[1], I.F. Schneider[2,3], M. Raoult[4], C. Strömholm[2], M. Larsson[5], and A. Suzor-Weiner[4,6,a]

[1] Faculty of Physics, Bucharest University, 76900 Bucharest, Romania
[2] Department of Physics I, Royal Institute of Technology (KTH), S-100 44 Stockholm, Sweden
[3] National Institute of Laser, Plasma and Radiation Physics, 76900 Bucharest, Romania
[4] Laboratoire de Photophysique Moléculaire, Université Paris-Sud, 91405 Orsay, France
[5] Department of Physics, Stockholm University, PO Box 6730, S-113 85 Stockholm, Sweden
[6] Laboratoire de Chimie Physique, Université Paris 6, 75231 Paris, France

Received: 18 September 1997 / Revised in final form: 17 October 1997 / Accepted: 20 October 1997

Abstract. The effect of rotational interaction in the low energy dissociative recombination process of diatomic molecules has been explored for typical molecular ions (H_2^+, HD^+, OH^+ and NO^+) which sample a large range of molecular masses. We show that rotation plays a role mainly for the indirect recombination process through bound Rydberg states, and for light molecules. When the direct process based on a strong electronic interaction is fast and dominating, rotational couplings can be safely neglected especially for heavier molecules like NO.

PACS. 31.50.+w Excited states – 31.70.-f Effects of atomic and molecular interactions on electronic structure – 34.80.Gs Molecular excitation and ionization by electron impact – 34.80.Kw Electron-ion scattering; excitation and ionization

1 Introduction

In the past five years the Dissociative Recombination (DR) of molecular ions has been actively studied, both experimentally and theoretically. The fundamental motivation is the importance of this process in cold ionised media (ionosphere, planetary atmospheres, interstellar matter) but the recent impulse comes from the ion storage ring experiments (see *e.g.* the review papers [1] and [2]) where molecular ions can be stored for several seconds and cooled by electronic collisions, thus allowing high resolution measurements of cross sections and branching ratios for fully relaxed ions. On the theoretical side, most of recent DR studies, using either time-dependent propagations [3], the R-matrix approach [4] or the Multichannel Quantum Defect Theory (MQDT) [5–7] have disregarded the effects of molecular rotation, assuming that the molecule has no time to rotate during the recombination process based on the different time scales for electronic, vibrational and rotational transitions. Either the rotational quantum numbers were neglected, or the *initial* rotational excitation of the molecular ion was assumed to be conserved during the whole process and passed to the neutral molecule, bound or dissociative [8]. This is obviously not rigorous since the colliding electron also carries angular momentum which should be properly combined with the initial angular momentum of the target ion. Accurate account of these rotational couplings have now been included in the theoretical treatment of DR within the MQDT approach but calculations have only been performed for the lighter molecular ions H_2^+ [9,10] and HD^+ [11,12].

In this short paper we try to answer the question: when will rotational couplings significantly affect the rate coefficient for dissociative recombination? We have performed numerical exploration for four diatomic molecular ions with reduced masses ranging from $0.5(H_2^+)$ to 7.5 (NO^+) see Table 1 — and we propose a practical criterion for predicting the effect of rotational interaction. The molecular mass largely determines the rotational structure and we have chosen a representative range for the most abundant diatomic ions in ionospheric or interstellar matter. Our exploration is restricted to low energy because previous calculations [12] have shown that rotational effects become negligible for recombination with fast electrons, even for the lightest molecular ions.

In Section 2 we give a brief outline of the theory, recalling how rotational couplings are included in the MQDT approach to DR. Section 3 describes the specific examples we have chosen and gives some numerical details. In Section 4 we summarize the results and discuss the practical criterion we can extract from these case studies.

[a] e-mail: annick@ppm.u-psud.fr

Table 1. Spectroscopic constants for the ground state ions involved in the present dissociative recombination calculations (from Huber and Herzberg [29]).

Ion	H_2^+	HD^+	OH^+	NO^+
Reduced mass (amu)	0.504	0.672	0.948	7.466
$\omega_e(cm^{-1})$	2321.7	1913.1	3113.37	2376.72
$B_e(cm^{-1})$	30.21	22.45	16.79	1.997

2 Summary of the theoretical approach

The inclusion of rotational interactions into the MQDT treatment of DR has been described recently [9,12] and is briefly summarised here.

We restrict the description to cases where DR may occur through electronic interaction between the {ion + incoming electron} initial configuration and a doubly excited state "d" whose dissociative potential curve crosses that of the ion initial state (exceptions like HeH^+ will be discussed later). The so-called "direct" DR mechanism results from this interaction and leads to a relatively smooth cross-section decreasing roughly as E^{-1}. A resonance structure is generally superimposed on this smooth variation and results from electron capture in excited ro-vibrational levels of bound Rydberg states, which are then predissociated by the same doubly excited state responsible for the direct process. This "indirect" mechanism [13] involves non-adiabatic couplings (vibrational and rotational) in the capture step. The direct and indirect processes happen and must be treated simultaneously [14] leading to Fano-type interference pattern [15] in the total cross section.

Including rotational interaction in the MQDT first means increasing the number of ionisation channels, labelled by new angular momentum quantum numbers. Starting from a given rovibrational level (N_i^+, v_i^+) of the ion initial electronic state, several values N of the total angular momentum of the neutral molecule can be formed by coupling with a specific partial wave l of the incoming electron. Each N value is a good quantum number conserved during the whole process and is involved in a separate calculation, leading to partial DR cross sections which are then summed to yield the total cross section:

$$\sigma_{d\leftarrow N_i^+ v_i^+} = \sum_N \sigma^{(N)}_{d\leftarrow N_i^+ v_i^+}. \quad (1)$$

Within each N subspace, rotation is included through a frame transformation [16,17] between coupling schemes corresponding to the incident electron being decoupled from (external region) or coupled to (internal region) the core electrons. The frame transformation mixes the different Λ quantum numbers compatible with a given set of $(N_i^+,\ l,\ N)$ values. The channel mixing coefficients involve angular coupling coefficients combined with electronic and vibrational factors:

$$\mathcal{C}_{\ell N_i^+ v_i^+,\ \Lambda\alpha} = \left(\frac{2N^+ + 1}{2N + 1}\right)^{1/2} \langle \ell(\Lambda - \Lambda^+) N^+ \Lambda^+ \left| \ell N^+ N \Lambda \right\rangle \times \frac{1 + \tau^+\tau(-1)^{N-\ell-N^+}}{[2(2-\delta_{\Lambda^+,0})(1+\delta_{\Lambda^+,0}\delta_{\Lambda,0})]^{1/2}} \times \sum_v \mathbf{U}^{\Lambda}_{\ell v,\alpha} \langle \chi_{N^+,v^+} \left| \cos\{\pi\mu_{\ell\Lambda}(R) + \eta^{\Lambda}_{\alpha}\} \right| \chi^{\Lambda}_{Nv} \rangle \quad (2)$$

$$\mathcal{C}_{d,\Lambda\alpha} = \mathbf{U}^{\Lambda}_{d,\alpha} \cos\eta^{\Lambda}_{\alpha} \quad (3)$$

as well as $\mathcal{S}_{N^+\ell v^+,\Lambda\alpha}$ and $\mathcal{S}_{d,\Lambda\alpha}$, obtained from equations (2, 3) by replacing "cos" by "sin". The $\chi_{N^+v^+}$ and χ^{Λ}_{Nv} are the vibrational wave functions of the ground state molecular ion in the $(N^+,\ v^+)$ rovibrational level and of a Rydberg monoexcited state in the $(N^+,\ v^+)$ rovibrational level and of a Rydberg monoexcited state in the $(N,\ v)$ rovibrational level respectively, and $\mu_{\ell\Lambda}(R)$ is the electronic quantum defect characterising these $l\Lambda$ — Rydberg series. For a given Λ, the index α denotes the eigenchannels defined through the diagonalization of the electronic reaction sub-matrix K^{Λ}, with eigenvalues and eigenvectors $-\frac{1}{\pi}\tan(\eta^{\Lambda}_{\alpha})$, and eigenvectors $(\mathbf{U}^{\Lambda}_{lv,\alpha}\ \mathbf{U}^{\Lambda}_{d,\alpha})$. Each block K^{Λ} of the reaction matrix is evaluated from the electronic coupling functions $V^{\Lambda}(R)$ between singly and doubly excited configurations with Λ symmetry, using a second order perturbative approach [18]. The quantities τ^+ and τ (with values ±1) are related to the reflection symmetry of the ion and neutral wave function respectively, and take the values $+1$ for symmetric states and -1 for antisymmetric ones [17]. The ratio in front of the sum in the right hand side of equation (2) contains the selection rules for the rotational quantum numbers. This factor, which results from the symmetrization of the wave functions, was not explicitly displayed in the preceding papers [9,12], but was taken into account in our calculations.

These channel mixing coefficients allow to compute the scattering matrix S restricted to open channels and containing the resonance structure, once the closed channels have been eliminated following the MQDT procedure of Seaton [19]. Finally, the partial cross sections in the sum of equation (1) are given by:

$$\sigma^{(N)}_{d\leftarrow N_i^+ v_i^+} = \frac{\pi\hbar^2}{4m_e\varepsilon}\rho\frac{2N+1}{2N_i^+ + 1}\sum_{\ell}\left|S^{(N)}_{d\leftarrow \ell N_i^+ v_i^+}\right|^2 \quad (4)$$

where ε is the energy of the incident electron, m_e the electron mass and ρ is the multiplicity ratio between the neutral and the ionic electronic states.

3 Case studies

Cross sections have been calculated for energies of the incident electron ranging from 0.02 meV to 0.6 eV, on a grid of 0.02 meV, narrow enough for most of the Rydberg resonances to be accounted. The initial rotational quantum number was $N_{\rm i}^+ = 2$ for all the calculations, because it is one of the most populated levels at room temperature and it is the lowest rotational quantum number allowed for one of our test cases (OH^+ in the $a^1\Delta$ initial state). Table 1 indicates the molecular ions selected for these test calculations, with their mass and ground state rotational constant.

We have performed calculations corresponding to three stages of complexity of our approach. First, we evaluate the direct rotation-free mechanism. Second, we allow for the indirect process, still neglecting the rotational couplings, *i.e.* total process but rotation-free calculations. And third, the total process with rotational structure and couplings included is considered. Since a relevant comparison between the total cross sections is difficult due to narrow resonance structure, we have evaluated the Maxwell rate coefficient in each case. Thus, the integrated effect of the rotational coupling is apparent from the comparison between the resulting smooth curves. Furthermore, very often it is the rate coefficient which is the relevant quantity for a kinetic calculation, rather than the cross section.

We present now the various DR reactions we have selected for this exploration and describe for each case the electronic states involved and our choice of molecular data.

3.1 H_2^+ and HD^+ dissociative recombination

We have studied the typical low-energy reaction

$$\begin{aligned} &H_2^+ \left\{X^2\Sigma_g^+,\ N_i^+ = 2,\ v_{\rm i}^+ = 0\right\} + e^-(l = 0,\ 2) \\ &\quad \longrightarrow H_2^{**} \left\{(2p\sigma_u)^2\ {}^1\Sigma_g^+\right\} \longrightarrow H + H^* \\ &\quad H_2^* \begin{Bmatrix} (X^2\Sigma_g^+)nl\sigma_g\ {}^1\textstyle\sum_g^+ \\ (X^2\Sigma_g^+)nd\pi_g\ {}^1\Pi_g \\ (X^2\Sigma_g^+)nd\delta_g\ {}^1\Delta_g \end{Bmatrix} \end{aligned} \tag{5}$$

and the similar one for HD^+, where only the "*s*" ($l = 0$) and "*d*" ($l = 2$) partial waves, giving the dominant contribution to DR, have been considered. The relevant potential curves for the ion and the neutral dissociative state are shown in Figure 1. The molecular data used have been selected from various structure or collision calculations [20–22]. Singly excited states of Σ, Π and Δ symmetry are included but for the three components of the d-complex (series dσ, dπ, dδ) we have adopted the same quantum defect function $\mu_{{\rm d}\sigma}({\rm R})$. This approximation, also made later for the p-complex in the OH and NO molecules due to lack of molecular data, amounts to neglect part of the direct rotational interaction [16], but in the presence of the strong electronic interaction prevailing in our DR examples the various N^+ channels are primarily mixed by indirect electronic couplings, as we have checked numerically.

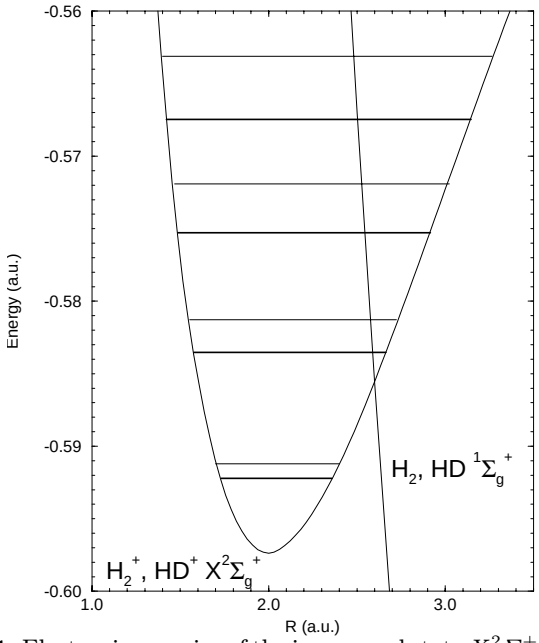

Fig. 1. Electronic energies of the ion ground state $X^2\Sigma_g^+$ of H_2^+ or HD^+ and of the lowest dissociative state $(2p\sigma_u)^2\ {}^1\Sigma_g^+$ of H_2 or HD. The $v^+ = 0-3$ vibrational levels of H_2^+ (corresponding to $N^+ = 2$) are shown with light lines, those of HD^+ with bold lines.

The resulting cross sections and Maxwell rate coefficients are displayed in Figure 2 for H_2^+ and in Figure 3 for HD^+.

3.2 OH^+ dissociative recombination

According to Guberman [6], the DR of OH^+ is dominated at low energy by the $2^2\Pi$ route. We have considered two different electronic states $X^3\Sigma^-$ and $a^1\Delta$ for the ionic target and only the p partial wave of the incident electron, giving rise to the reactions:

$$\begin{aligned} &OH^+ \left\{X^3\Sigma^- N_{\rm i}^+ = 2,\ v_{\rm i}^+ = 0\right\} + e^-(l = 1) \\ &\quad \longrightarrow OH^{**} \left\{2^2\Pi\right\} \longrightarrow \begin{cases} O^* + H \\ O + H^* \end{cases} \\ &\quad OH^* \begin{Bmatrix} (X^3\Sigma^-)\ np\pi\ {}^2\Sigma \\ (X^3\Sigma^-)\ np\sigma\ {}^2\Pi \end{Bmatrix} \end{aligned} \tag{6}$$

and:

$$\begin{aligned} &OH^+ \left\{a^1\Delta\ N_{\rm i}^+ = 2,\ v_{\rm i}^+ = 0\right\} + e^-(l = 1) \\ &\quad \longrightarrow OH^{**} \left\{2\ {}^2\Pi\right\} \longrightarrow \begin{cases} O^* + H \\ O + H^* \end{cases} \\ &\quad OH^* \begin{Bmatrix} (a^1\Delta)\ np\pi\ {}^2\Pi \\ (a^1\Delta)\ np\sigma\ {}^2\Delta \\ (a^1\Delta)\ np\pi\ {}^2\Phi \end{Bmatrix}. \end{aligned} \tag{7}$$

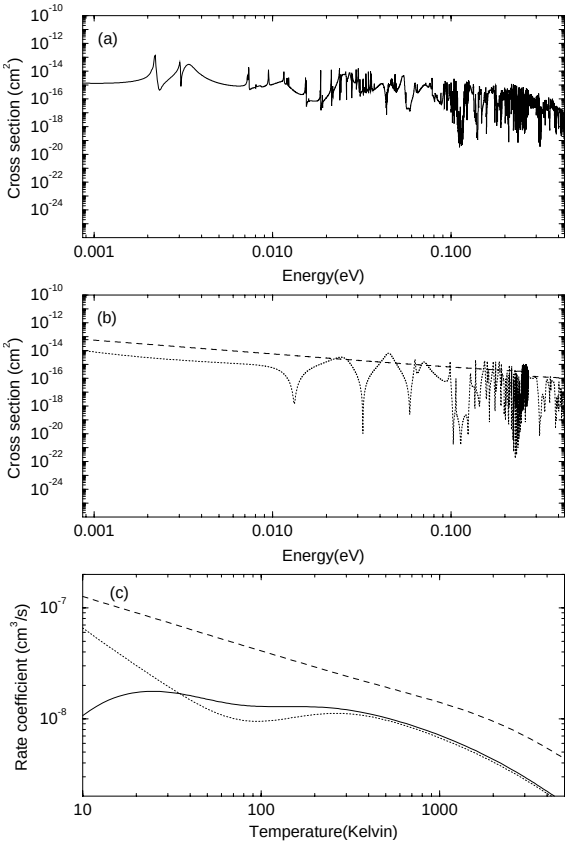

Fig. 2. Rotational effects in the dissociative recombination of H_2^+ ($X^2\Sigma_g^+$, $N_i^+ = 2$, $v_i^+ = 0$) *via* the dissociative state $H_2(2p\sigma_u)^2\ ^1\Sigma_g^+$: (a) cross section, rotational calculations; (b) cross sections, rotation-free calculations: *dotted lines* for total process and *dashed lines* for direct process only; (c) Maxwell rate-coefficients: *continuous lines* for rotational calculations, *dotted lines* for total process, rotation-free calculations and *dashed lines* for direct process, rotation-free calculations.

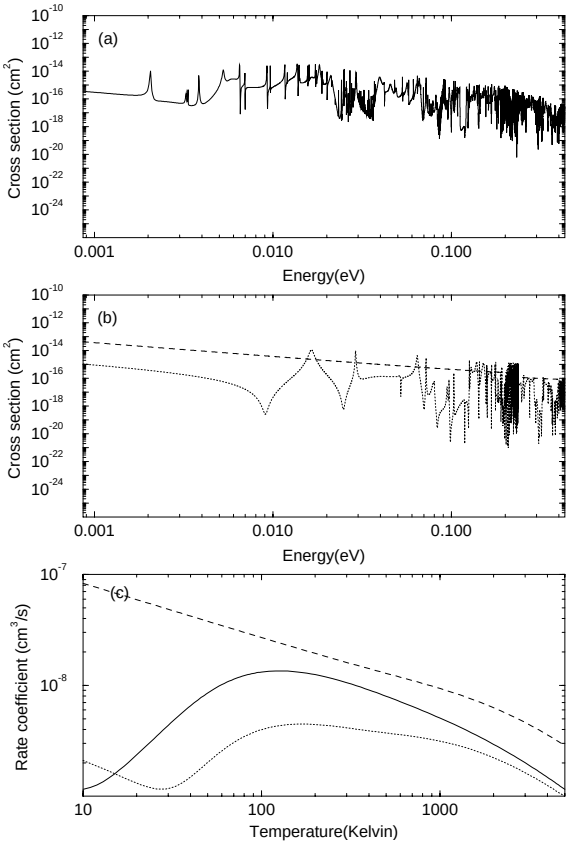

Fig. 3. Same as in Figure 2, for HD^+/HD.

Molecular data are the same as for previous calculations [23] and have been calculated by Guberman [6] and Hirst and Guest [24]. The relevant potential curves are displayed in Figure 4 and the results of the calculations are given in Figure 5 for the $X^3\Sigma^-$ initial ion state, and in Figure 6 for the ion being initially in the metastable $a^1\Delta$ state.

3.3 NO^+ dissociative recombination

Numerous spectroscopic studies [25] followed by theoretical analysis of the dynamics of high Rydberg states in NO [26,27] indicate that the low-energy dissociative recombination of NO^+, initially in its ground state $X^1\Sigma^+$, can occur through several dissociative states of the neutral molecule, among which $B^2\Pi$ and $L^2\Pi$. Following previous calculations by Sun and Nakamura [28], we treat

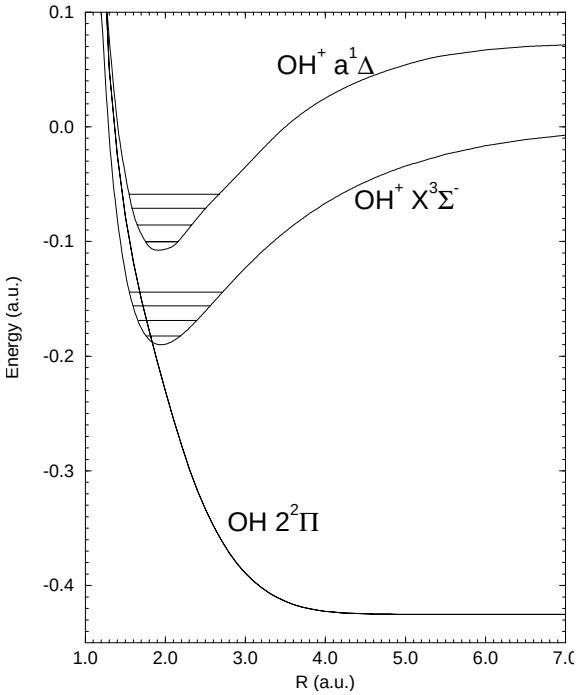

Fig. 4. Electronic energies for $OH^+(X^3\Sigma^-)$ and $OH^+(a^1\Delta)$ from [23], and for $OH(2^2\Pi)$ from [6]. Also shown are the vibrational levels of the molecular ion states corresponding to $N^+ = 2$.

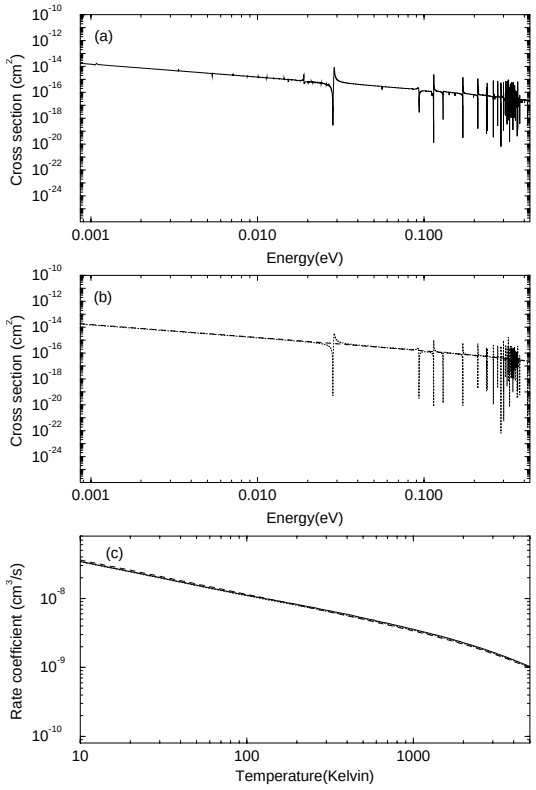

Fig. 5. Rotational effects in the dissociative recombination of $OH^+(X^3\Sigma^-,\ N_i^+ = 2,\ v_i^+ = 0)$ *via* the OH $(2^2\Pi)$ dissociative state: (a) cross section, rotational calculations; (b) cross sections, rotation-free calculations: *dotted lines* for total process and *dashed lines* for direct process only; (c) Maxwell rate-coefficients: *continuous lines* for rotational calculations, *dotted lines* for total process, rotation-free calculations and *dashed lines* for direct process, rotation-free calculations.

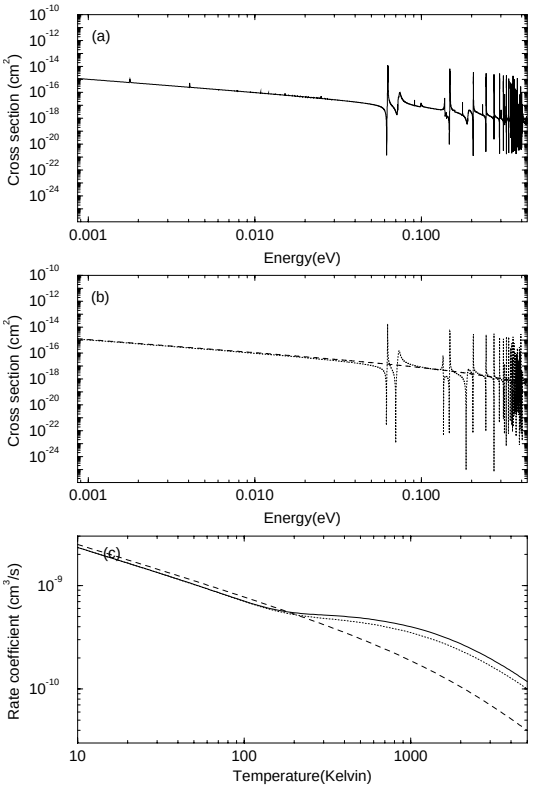

Fig. 6. Same as in Figure 5, for initial state $OH^+(a^1\Delta,\ N_i^+ = 2,\ v_i^+ = 0)$.

successively the two reactions:

$$\begin{aligned} &NO^+\left\{X^1\Sigma^+ N_i^+ = 2,\ v_i^+ = 0\right\} + e^-(l=1) \\ &\quad\longrightarrow NO^{**}\left\{B\ ^2\Pi\right\} \longrightarrow \begin{cases} N^* + O \\ N + O^* \end{cases} \\ &\quad NO^*\begin{Bmatrix} (X^1\Sigma^+)\ np\pi\ ^2\Pi \\ (X^1\Sigma^+)\ np\sigma\ ^2\sum \end{Bmatrix} \end{aligned} \tag{8}$$

and:

$$\begin{aligned} &NO^+\left\{X^1\Sigma^+ N_i^+ = 2,\ v_i^+ = 0\right\} + e^-(l=1) \\ &\quad\longrightarrow NO^{**}\left\{L\ ^2\Pi\right\} \longrightarrow \begin{cases} N^* & +O \\ N & +O^* \end{cases} \\ &\quad NO^*\begin{Bmatrix} (X^1\Sigma^+)\ np\pi\ ^2\Pi \\ (X^1\Sigma^+)\ np\sigma\ ^2\sum \end{Bmatrix} \end{aligned} \tag{9}$$

Note that an accurate calculation should include these two dissociative states of same symmetry simultaneously as we did *e.g.* for HD^+ calculations [2,12], but for our present purpose it is more demonstrative to look at their separate contribution.

The molecular data have been obtained by Raoult [27] and the relevant potential curves are shown in Figure 7. As in the case of OH^+ DR, only the "p" partial wave of the incident electron is accounted for. The final results are given in Figure 8 for the contribution of the $B^2\Pi$ dissociative state, and in Figure 9 for that of the $L^2\Pi$ state.

4 Discussion and interpretation of the results

The results of the set of calculations presented in Section 3 are summarised in Figure 10. They clearly show that the importance of rotational effects depends on the molecular mass, but even more on the weight of the indirect process in the total cross section. In previous studies on light ions [9,12] it was already demonstrated that rotational effects are small for the direct process, but can be important for the total cross section and seems to be correlated with the effect of Rydberg resonances. In fact, this is to be expected, since resonant capture into bound monoexcited Rydberg states is due to non-adiabatic interaction between the continuum and Rydberg configurations. The shape of the corresponding resonances in the cross section can be interpreted in terms of the Fano q-parameter [15], proportional in our case to the strengths of this interaction.

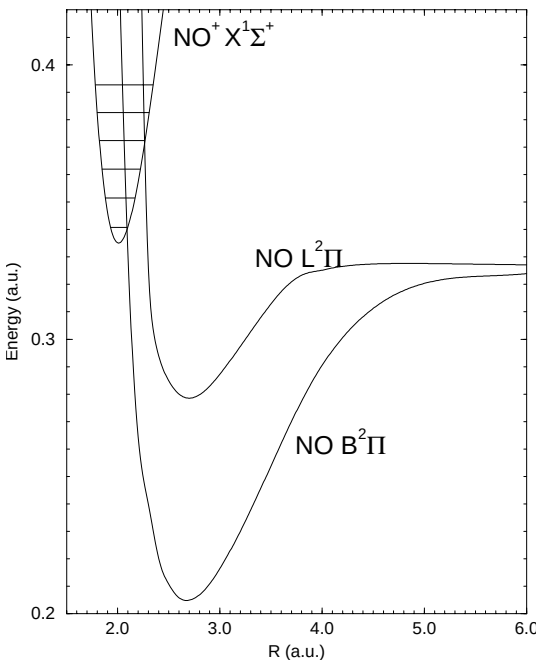

Fig. 7. Electronic energies for $NO^+(X^1\Sigma^+)$, NO ($B^2\Pi$) and NO ($L^2\Pi$) states from [26] and vibrational levels of the molecular ion corresponding to $N^+ = 2$.

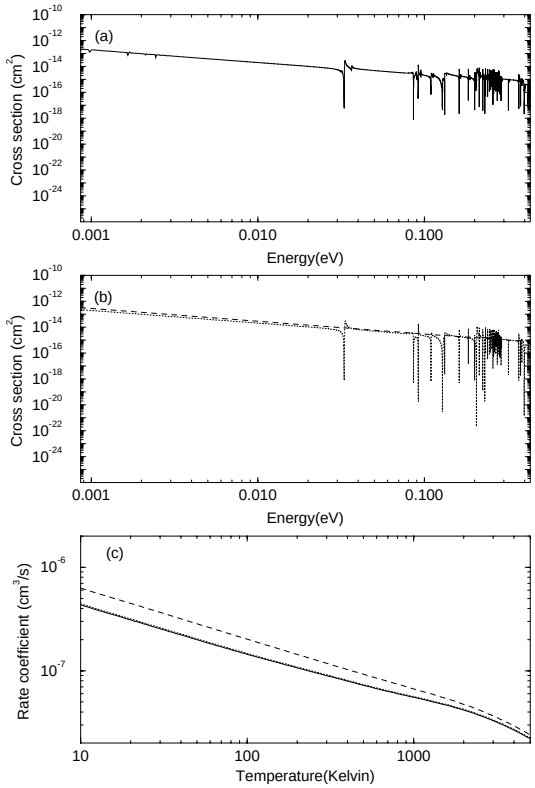

Fig. 8. Rotational effects in the dissociative recombination of $NO^+(X^1\Sigma^+,\ N_i^+ = 2,\ v_i^+ = 0)$ *via* the NO ($B^2\Pi$) valence state: (a) cross section, rotational calculations; (b) cross sections, rotation-free calculations: *dotted lines* for total process and *dashed lines* for direct process only; (c) Maxwell rate-coefficients: *Continuous lines* for rotational calculations, *dotted lines* for total process, rotation-free calculations and *dashed lines* for direct process, rotation-free calculations.

The most apparent effect of including the rotational couplings is to increase the number of ionisation channels, in particular of *closed* channels (with ionisation threshold above the total energy) which bring new Rydberg resonances in the cross section (compare for example Figs. 2a and 2b, or 3a and 3b). In most of our examples these new resonances result in an increase of the rate coefficient with respect to the rotation-free value. This is due to the inclusion of an additional capture mechanism, through non-adiabatic angular interaction between the continuum and Rydberg states, which slightly changes the resonance profile in favour of larger values for the Fano q-parameter. According to [15], this corresponds to more constructive interferences between direct and indirect DR process, *i.e.* to resonances with smaller dips and higher peaks, resulting in larger averaged cross sections and rates. The rotational couplings being proportional to the rotational constant, the effect is generally stronger for light molecules, as is clear in Figure 10. Note however that this mass effect is only valid for large mass differences, like going from HD^+ to NO^+, but for small differences (*e.g.* between H_2^+ and HD^+) it may be dominated by other factors discussed below.

Since the effect of rotational couplings is clearly correlated with the indirect process, it is interesting to analyse when and why the resonant mechanism plays an important role in the DR process. Inspection of our examples shows that the width and amplitude of the Rydberg resonances depend mainly on the relative position of the ion curve and the dissociative (neutral) one. If these curves cross within the Franck-Condon region of the initial ion vibrational level, the direct process will be fast and the indirect one relatively weak. If on the contrary the dissociative curve does not cross the ion curve, or crosses it closer to the Franck-Condon region of an excited vibrational level corresponding to a closed ionization channels, then the Rydberg resonances play an important role and the rotational effects become appreciable. These contrasted situations are illustrated in our examples:

- first, we can understand why the rotational effects are larger for HD^+ DR than for H_2^+: Figure 1 shows that the crossing between the ion curve and the dissociative one is closer to the first excited level of HD^+ than of H_2^+. This results in a larger amplitude for the $v = 1$ resonances, and thus in a larger contribution of the rotational interactions;
- using the same argument, we can understand why in the case of OH^+ the rotational effect is stronger (with a maximum of 20% instead of 4%) when the ion is in the excited state $a^1\Delta$ (reaction 7) than of the ground state $X^3\Sigma^-$ (reaction 6): the crossing of the (same) dissociative curve with the ion curve favours the closed channels in the former case, corresponding to excited vibrational levels, and the open $v = 0$ channel in the latter case;

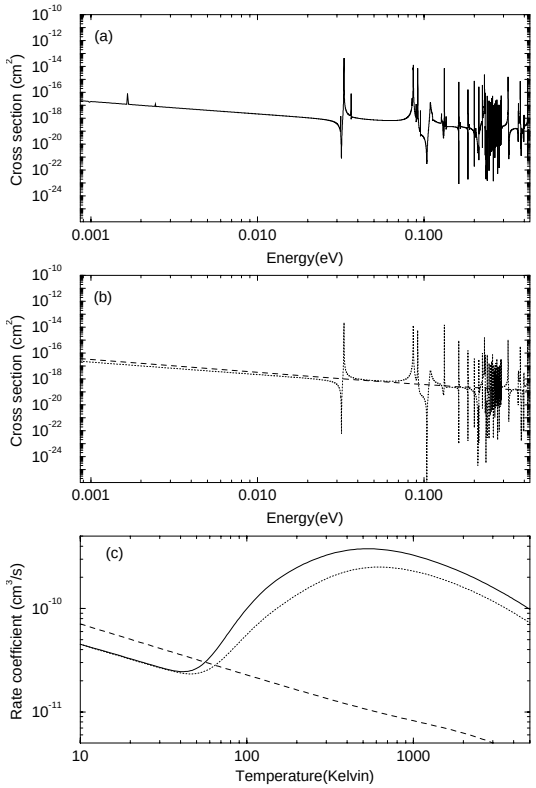

Fig. 9. Same as in Figure 8, for the contribution of the valence state NO ($L^2\Pi$) to the $NO^+(X^1\Sigma^+,\ N_i^+ = 2,\ v_i^+ = 0)$ dissociative recombination.

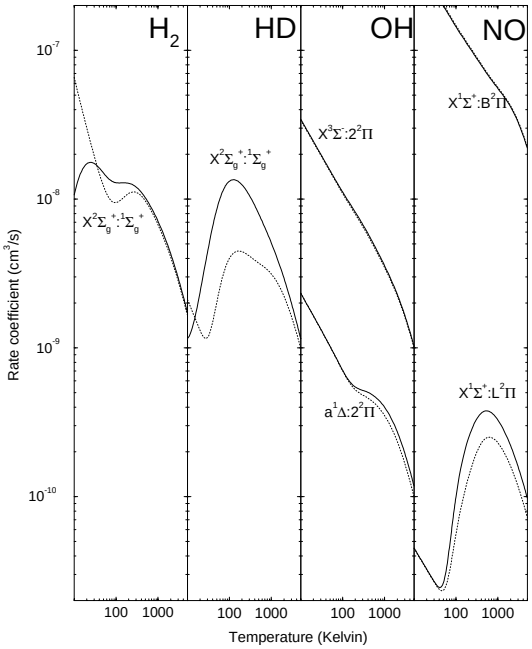

Fig. 10. Summary of rotational effects for the 4 ions studied. The rate coefficients for the total (direct + indirect) process are displayed, with full line for the rotational treatment and dashed line for the rotation-free calculations. The initial rotational level is $N_i^+ = 2$ and the initial vibrational level is $v_i^+ = 0$. The electronic state of the target ion and that of the dissociative state of the neutral system are indicated in each case.

– finally, the most striking illustration is given by the B and L dissociative states involved in the low energy DR of NO^+ ground state (Eqs. (8 and 9)). The $B^2\Pi$ curve crosses the ion ground state not far from the equilibrium distance (see Fig. 7) and gives rise to a large $v_i^+ = 0$ cross section dominated by the direct recombination, with narrow and weak Rydberg resonances (Figs. 8a, 8b). On the contrary, the $L^2\Pi$ state has a much better overlap with the excited vibrational ion levels, which leads to more prominent resonance structure (Figs. 9a, 9b). It is clear from Figure 10 that rotational effects are negligible in the former case (less than 2%) but important for the contribution of the L state (up to 90%, see [30]). This contribution is too weak anyway to affect the total rate for $v_i^+ = 0$, but this demonstrates that for a slow DR reaction, rotation may have an effect even for relatively heavy molecular ions.

From this analysis, we can infer a practical criterion, within the non-rotational approach, which may help to determine if rotational interactions should be included in a specific rate calculation. Indeed, the contribution of the indirect process may be measured from the difference between the Maxwell rate coefficients for the rotation-free direct and total DR processes. Among the seven calculations presented in Section 3, only three correspond to differences larger than 80% between rates for direct and total DR (HD^+, H_2^+ and the L-state contribution to NO^+ DR), and only for these three cases the rotational effect is larger than 40%.

Based on this criterion, a good candidate for appreciable rotational effects is HeH^+ recombining with slow electrons. Indeed, the absence of a low-lying doubly excited dissociative state crossing the ion ground state leads to a relatively weak direct DR process, entirely due to non-adiabatic couplings [4,5]. By taking account of the Ryberg resonances and all the *radial* interchannel couplings, the order of magnitude of the fast DR rate measured in various experiments could be reproduced and Guberman [5] pointed out the prominent role of the indirect process, which may change the cross section by up to two orders of magnitude. Thus it seems likely that rotational effects, in this light molecule with important indirect DR, could notably contribute to the process.

5 Conclusion

The magnitude of the effect of the rotational coupling depends on the molecular mass and on the position of the crossing between the ion and dissociative electronic curves with respect to the initial vibrational level. The effects are appreciable when the crossing corresponds to a weak Franck-Condon overlap, and for light molecules. For equally favourable crossings, the effect decreases when the molecular mass increases.

A practical criterion for estimating the importance of the rotational coupling consists in comparing the rates for the direct and global DR processes, in the rotation-free case. The relative importance of the indirect (resonant) process is a good indication for the change in the cross section when one passes from rotation-free to rotational calculations. We can thus predict the effect of the rotational couplings based on the strength of the indirect process in the rotation-free treatment. This also explains why they are negligible at high energy, above the ion dissociation limit, where no more non-adiabatic capture into bound Rydberg states may occur. Although our tests have been restricted to diatomic ions, it is likely that this conclusion can be extended to polyatomic ions.

We conclude by emphasizing that only the effect of rotational interactions (possibly leading to rotational excitation or desexcitation) *during* the DR process has been explored here, not that of initial rotational excitation of the ion. The rotational population usually follows a Boltzmann distribution, both in natural environments and in the ion tube of storage rings, and the rate may change appreciably from low to high *initial* rotational levels. As long as one may assume that the rotation quantum number N_i^+ is conserved during the whole process, the theoretical treatment is analogous to the rotation-free case except for additional centrifugal potential, but a new calculation has to be performed for each N_i^+ value to allow the Boltzmann averaging.

This work has been supported by the Göran Gustafsson Foundation and by the HCM programme of EC, under contract ERB 4050PL94-1414. B.V. acknowledges a TEMPUS grant from EC. We thank S. Guberman for having communicated unpublished molecular data for the OH radical, and for helpful comments on the manuscript.

References

1. P. Fork, M. Grieser, D. Habs, A. Lampert, R. Repnow, D. Schwalm, A. Wolf, D. Zajfman, Nucl. Instrum. Methods Phys. Rev. B **79**, 273 (1993).
2. M. Larsson, Phys. World **9**, 40 (1996); M. Larsson, Ann. Rev. Phys. Chem. **48**, 145 (1997).
3. A.E. Orel, K.C. Kulander, T.N. Rescigno, Phys. Rev. Lett. **74,**, 4807 (1995).
4. B.K. Sarpal, J. Tennyson, L.A. Morgan, J. Phys. B **27**, 5943 (1994).
5. S.L. Guberman, Phys. Rev. A **49**, R4277 (1994).
6. S.L. Guberman, J. Chem. Phys. **102**, 1699 (1995).
7. C. Strömholm, I.F. Schneider, G. Sundström, L. Carata, H. Danared, S. Datz, O. Dulieu, A. Källberg, M. af Uglas, X. Urbain, V. Zengin, A. Suzor-Weiner, M. Larsson, Phys. Rev. A **52**, R4320 (1995).
8. I.F. Schneider, O. Dulieu, A. Giusti-Suzor, E. Roueff, Astrophys. J. **424**, 983 (1994).
9. H. Takagi, J. Phys. B **26**, 4815 (1993).
10. G.V. Golubkov, M.G. Golubkov, G.K. Ivanov, Zh. Eksp. Teor. Fiz. **108** 105 (1995); Engl. Transl. Sov. Phys.-JETP **81**, 56 (1995).
11. T. Tanabe, I. Katayama, N. Inoue, K. Chida, Y. Arakaki, T. Watanabe, M. Yoshisawa, S. Ohtani, K. Noda, Phys. Rev. Lett. **75**, 1066 (1995).
12. I.F. Schneider, C. Strömholm, L. Carata, X. Urbain, M. Larsson, A. Suzor-Weiner, J Phys. B **30**, 2687 (1997).
13. J.N. Bardsley, J. Phys. B **1**, 365 (1968).
14. A. Giusti, J. Phys. B **13**, 3687 (1980).
15. U. Fano, Phys. Rev. **124**, 1866 (1961).
16. U. Fano, Phys. Rev. A **2**, 353 (1970) .
17. E.S. Chang, U. Fano, Phys. Rev. A **6**, 173 (1972) .
18. S.L. Guberman, A. Giusti-Suzor, J. Chem. Phys. **95**, 2602 (1991).
19. M.J. Seaton, Rep. Prog. Phys. **46**, 167 (1983) .
20. L. Wolniewicz, K. Dressler, J. Chem. Phys. **82**, 3292 (1985).
21. L.A. Collins, B. Schneider, D.L. Lynch, C.J. Noble, Phys. Rev. A **52**, 1310 (1995).
22. J. Tennyson, At. Data Nucl. Data Tables **64**, 253 (1996).
23. C. Strömholm, H. Danared, A. Larsson, M. Larsson, C. Marian, S. Rosen, B. Schimmelpfennig, I.F. Schneider, J. Semaniak, A. Suzor-Weiner, U. Wahlgren, Van der Zande, J. Phys. B (in press 1997).
24. D. Hirst, M. Guest, Molecular Physic **49**, 1461-1469 (1983) .
25. E. Miescher, Can. J. Phys. **54**, 2074 (1976).
26. A. Giusti-Suzor, Ch. Jungen, J. Chem. Phys. **80**, 986 (1984).
27. M. Raoult, J. Chem. Phys. **87**, 4736 (1987) .
28. H. Sun, H. Nakamura, J. Chem. Phys. **93**, 6491 (1990) .
29. K.P. Huber, G. Herzberg, in *Molecular Spectra and Molecular Structure IV* (Van Nostrand Reinhold Company, New York, 1979).
30. The difference between the rate coefficients for direct (dashed line) and total (dotted line) processes in Fig. 9c may seem large when compared to the resonance structure in Fig. 9b above. This is due to the different scales between the two figures, and also to the logarithmic scales which make the resonances look almost symmetric in Fig. 9b while actually their positive parts are much larger than the dip ones and lead to an appreciable increase of the rate after Maxwell averaging.